J|A|C|S
ARTICLES
Published on Web 00/00/0000

GFT NMR, a New Approach To Rapidly Obtain Precise High-Dimensional NMR Spectral Information

Seho Kim† and Thomas Szyperski*

Contribution from the Department of Chemistry, University at Buffalo, The State University of New York, The Northeast Structural Genomics Consortium, Buffalo, New York 14260

Received August 19, 2002; E-mail: szypersk@chem.buffalo.edu

Abstract: Widely used higher-dimensional Fourier transform (FT) NMR spectroscopy suffers from two major drawbacks: (i) The minimal measurement time of an *N*-dimensional FT NMR experiment, which is constrained by the need to sample $N - 1$ indirect dimensions, may exceed by far the measurement time required to achieve sufficient signal-to-noise ratios. (ii) The low resolution in the indirect dimensions severely limits the precision of the indirect chemical shift measurements. To relax on constraints arising from these drawbacks, we present here an acquisition scheme which is based on the phase-sensitive joint sampling of the indirect dimensions spanning a subspace of a conventional NMR experiment. This allows one to very rapidly obtain high-dimensional NMR spectral information. Because the phase-sensitive joint sampling yields subspectra containing "chemical shift multiplets", alternative data processing is required for editing the components of the multiplets. The subspectra are linearly combined using a so-called "*G*-matrix" and subsequently Fourier-transformed. The chemical shifts are multiply encoded in the resonance lines constituting the shift multiplets. This corresponds to performing statistically independent multiple measurements, and the chemical shifts can thus be obtained with high precision. To indicate that a combined *G*-matrix and FT is employed, we named the new approach "GFT NMR spectroscopy". GFT NMR opens new avenues to establish high-throughput protein structure determination, to investigate systems with a higher degree of chemical shift degeneracy, and to study dynamic phenomena such as slow folding of biological macromolecules in greater detail.

Introduction

NMR[1] spectra need to exhibit (i) signal-to-noise (S/N) ratios warranting reliable data interpretation, (ii) digital resolutions ensuring adequate precision for the measurement of NMR parameters such as chemical shifts, and (iii) a dimensionality at which a sufficient number of NMR parameters is correlated.[2,3] Above a minimal "target dimensionality" N_t at which most of the peaks are resolved, increased dimensionality does not aim at resolving peak overlap but at increasing the number of correlations obtained in a single data set. This eliminates ambiguities when several multidimensional NMR spectra are combined for resonance assignment, for example, when using ^{1}H,^{13}C,^{15}N triple-resonance NMR to assign protein resonances.[3] An increase in dimensionality is, however, limited by the need to independently sample the indirect dimensions because this leads to longer measurement times. Although the measurement time can be somewhat reduced by aliasing signals[3] or accepting a lower digital resolution in the indirect dimensions, high dimensionality often prevents one from tuning the measurement time to a value that ensures one will obtain sufficient, but not unnecessarily large, S/N ratios.

In view of these considerations, "sampling" and "sensitivity limited" data collection regimes are defined[4] depending on whether the sampling of the indirect dimensions or the sensitivity of the FT NMR experiment determines the minimal measurement time. In the sensitivity limited regime, long measurement times are required to achieve sufficient S/N ratios, so that the sampling of indirect dimensions is not necessarily constraining the adjustment of the measurement time. In the sampling limited regime, some or even most of the instrument time is invested for sampling, which yields excessively large S/N ratios.[5] In view of the ever increasing sensitivity of NMR instrumentation, new methodology to avoid the sampling limited regime is needed.[4]

In general, phase-sensitive acquisition of an *N*D FT NMR experiment[2,3] requires sampling of $N - 1$ indirect dimensions with $n_1 \times n_2 \ldots n_{N-1}$ complex points representing $n_{\mathrm{FID}} = 2^{N-1} \cdot \prod_{j=1}^{N-1} n_j$ FIDs. The resulting steep increase of the minimal measurement time, T_{m}, with dimensionality prevents one from recording five- or higher-dimensional FT NMR spectra: acquir-

† Present address: Department of Chemistry, Rutgers University, Piscataway, NJ 08854.

(1) Abbreviations used: NMR, nuclear magnetic resonance; 1D, 2D, 3D, 4D, 5D, one-, two-, three-, four-, five-dimensional; FID, free induction decay; FT, Fourier transformation; GFT, combined *G*-matrix and Fourier transformation; NOE, nuclear Overhauser effect; COSY, correlation spectroscopy; NOESY, nuclear Overhauser enhancement spectroscopy; rf, radio frequency; DSS, 2,2-dimethyl-2-silapentane-5-sulfonate.

(2) Ernst, R. R.; Bodenhausen, G.; Wokaun, A. *Principles of Nuclear Magnetic Resonance in One and Two Dimensions*; Clarendon: Oxford, 1987.

(3) Cavanagh, J.; Fairbrother, W. J.; Palmer, A. G.; Skelton, N. J. *Protein NMR Spectroscopy*; Academic Press: San Diego, 1996.

(4) Szyperski, T.; Yeh, D. C.; Sukumaran, D. K.; Moseley, H. N. B.; Montelione, G. T. *Proc. Natl. Acad. Sci. U.S.A.* **2002**, *99*, 8009−8014.

10.1021/ja028197d CCC: $25.00 © xxxx American Chemical Society

ing 16 complex points in each indirect dimension (with one scan per FID each second) yields $T_m(3D) = 0.5$ h, $T_m(4D) = 9.1$ h, $T_m(5D) = 12$ days, and $T_m(6D) = 1.1$ years. Hence, new techniques are required which make five- or higher-dimensional spectral information accessible.

Here we present a generally applicable approach for data acquisition and processing named "GFT NMR spectroscopy". This approach is based on the phase-sensitive joint sampling of several indirect dimensions while ensuring that all chemical shift correlations are retained. The employment of GFT NMR focuses on the sampling limited data collection regime and, considering that NMR measurements longer than about a week are impracticable, on the acquisition of five- or higher-dimensional spectral information. In the sensitivity limited regime, GFT NMR may be advantageous in cases where an extended rf phase cycle is desirable for spectral editing and/or improved artifact suppression.[3]

Methods

Theory. In GFT NMR spectroscopy, the chemical shift evolution periods spanning a given multidimensional subspace of an FT NMR experiment are *jointly* sampled (Figure 1). Thereby, the dimensionality N of an FT NMR spectrum can be adjusted to a given target dimensionality, N_t, by combined sampling of $K + 1$ chemical shifts $\Omega_0, \Omega_1 \ldots \Omega_K$ encoded in $K + 1$ indirect dimensions of the ND FT NMR experiment ($K = N - N_t$). Assuming that Ω_0 is detected in quadrature[2] and that the setting of the phases ϕ_j of the radio frequency pulses exciting the spins of dimension j ($j = 1 \ldots K$) ensures cosine modulation, the transfer amplitude[2] of the N_tD experiment is proportional to $e^{i\Omega_0 t} \cdot \prod_{j=1}^{K} \cos(\Omega_j t)$. The resulting peak centered around Ω_0 contains 2^K components and shall be designated a "chemical shift multiplet" (Figure 2).

A shift of ϕ_j by 90° yields a $\sin(\Omega_j t)$ instead of a $\cos(\Omega_j t)$ modulation,[2] and 2^K N_tD spectra are to be recorded if all phases ϕ_k are systematically varied between 0° and 90° (Figure 1). In turn, a linear combination of these 2^K spectra allows for the editing of the chemical shift multiplet components (Figure 2). For brevity, we define $c_j = \cos(\Omega_j \cdot t)$, $s_j = \cos(\Omega_j \cdot t)$, and $e^{i\Omega_j t} = e^{i_j}$, so that

$$e^{i_j} = c_j + i \cdot s_j = \begin{bmatrix} 1 & i \end{bmatrix} \cdot \begin{bmatrix} c_j \\ s_j \end{bmatrix}$$

With $K = 1$, one obtains for the time evolution of the two shift multiplet components encoding the sum and difference of Ω_0 and Ω_1:

$$\begin{bmatrix} e^{i_1} \\ e^{-i_1} \end{bmatrix} \otimes e^{i_0} = \begin{bmatrix} e^{i_1} \cdot e^{i_0} \\ e^{-i_1} \cdot e^{i_0} \end{bmatrix} = \begin{bmatrix} e^{i_0 + i_1} \\ e^{i_0 - i_1} \end{bmatrix} = \begin{bmatrix} \begin{bmatrix} 1 & i \end{bmatrix} \otimes \begin{bmatrix} 1 & i \end{bmatrix} \\ \begin{bmatrix} 1 & -i \end{bmatrix} \otimes \begin{bmatrix} 1 & i \end{bmatrix} \end{bmatrix} \cdot \begin{bmatrix} \begin{bmatrix} c_1 \\ s_1 \end{bmatrix} \otimes \begin{bmatrix} c_0 \\ s_0 \end{bmatrix} \end{bmatrix} = \begin{bmatrix} \begin{bmatrix} 1 & i \\ 1 & -i \end{bmatrix} \otimes \begin{bmatrix} 1 & i \end{bmatrix} \end{bmatrix} \cdot \begin{bmatrix} \begin{bmatrix} c_1 \\ s_1 \end{bmatrix} \otimes \begin{bmatrix} c_0 \\ s_0 \end{bmatrix} \end{bmatrix}$$

(5) NMR-based structural studies rely on two classes of experiment. COSY delineates exclusively scalar coupling connectivities to measure chemical shifts, and (heteronuclear resolved) ^{1}H,^{1}H-NOESY reveals the strength of through-space dipolar couplings of ^{1}H spins to estimate distances.[2,3] While increased intensity of NOESY peaks ensures their more accurate integration (which in turn may translate into increased accuracy of the NMR structure), the mere identification of COSY peaks suffices to obtain the desired chemical shifts. Hence, COSY peak signal-to noise ratios larger that ~3:1 reflect, in essence, inappropriately long measurement times. Moreover, the total number of peaks in COSY grows only linearly with the number of spins involved and is, for a defined magnetization transfer pathway, *independent* of the dimensionality N. Hence, we have quite generally that the target dimensionality is given by $N_t = 2,3$ for COSY.

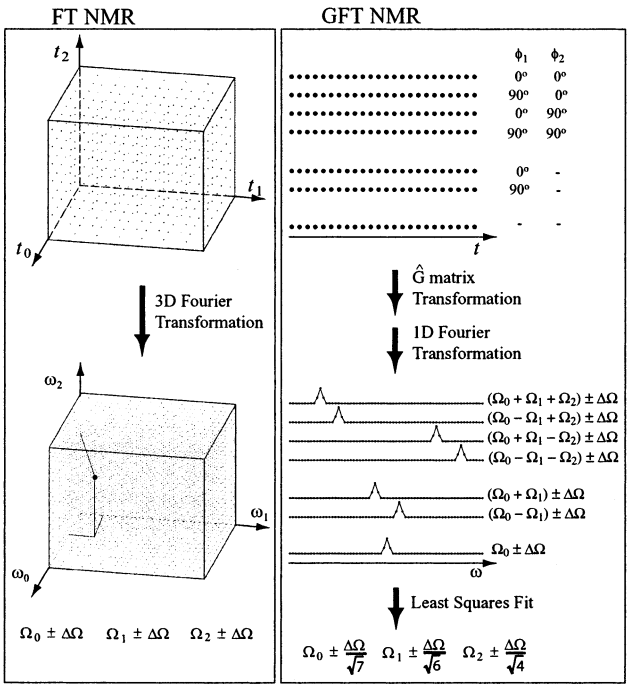

Figure 1. Comparison of the conventional sampling of a 3D time domain subspace of an ND FT NMR experiment (on the left) with the phase-sensitive joint sampling of the three dimensions in an (N,N-2)D GFT NMR experiment (on the right), that is, with $K = 2$ (see Theory section). Processing of the FT NMR experiment requires a 3D FT of the subspace, while the GFT NMR experiment requires time domain editing of chemical shift multiplet components by application of the so-called G-matrix (see eq 1 in the Theory section) and 1D FT of the resulting $p = 2^{K+1}$ data sets. For the GFT NMR experiment, the phase settings of ϕ_1 and ϕ_2 of the rf pulses creating transverse magnetization for frequency labeling with Ω_1 and Ω_2 are indicated for basic spectra (top four rows), first-order central peak spectra (two rows in the middle), and the second-order central peak spectrum (bottom row). Instead of a single peak in FT NMR which encodes three chemical shifts, one obtains a p-fold overdetermined system of equations. A least-squares fit calculation yields the three shifts from the position of seven peaks. In a GFT NMR experiment with constant-time chemical shift evolution periods (see text), the lines forming the chemical shift multiplets have the same width as the resonances in FT NMR (if recorded with corresponding maximal evolution times; see also Figure 7a,b).[12] This yields the same standard deviation $\Delta\Omega$ for the identification of peak positions in the two experiments. Hence, the standard deviation of the chemical shift measurements obtained *after* the least-squares fit is reduced[9] by a factor $1/\sqrt{n}$ in GFT NMR. For simplicity, it is assumed that the n peaks which contribute to the calculation of a given shift exhibit the same line widths (see text and also legends of Figures 8, S1).

Accordingly, one obtains with $K = 2$ for three chemical shifts Ω_0, Ω_1, and Ω_2:

$$\begin{bmatrix} e^{i_2} \\ e^{-i_2} \end{bmatrix} \otimes \begin{bmatrix} e^{i_1} \\ e^{-i_1} \end{bmatrix} \otimes e^{i_0} = \begin{bmatrix} \begin{bmatrix} 1 & i \\ 1 & -i \end{bmatrix} \otimes \begin{bmatrix} 1 & i \\ 1 & -i \end{bmatrix} \otimes \begin{bmatrix} 1 & i \end{bmatrix} \end{bmatrix} \cdot \begin{bmatrix} \begin{bmatrix} c_2 \\ s_2 \end{bmatrix} \otimes \begin{bmatrix} c_1 \\ s_1 \end{bmatrix} \otimes \begin{bmatrix} c_0 \\ s_0 \end{bmatrix} \end{bmatrix}$$

and, in general, for $K + 1$ chemical shifts $\Omega_0, \Omega_1, \ldots \Omega_K$:

$$\begin{bmatrix} e^{i_K} \\ e^{-i_K} \end{bmatrix} \otimes \ldots \otimes \begin{bmatrix} e^{i_1} \\ e^{-i_1} \end{bmatrix} \otimes e^{i_0} = \begin{bmatrix} \begin{bmatrix} 1 & i \\ 1 & -i \end{bmatrix} \otimes \ldots \otimes \begin{bmatrix} 1 & i \\ 1 & -i \end{bmatrix} \otimes \begin{bmatrix} 1 & i \end{bmatrix} \end{bmatrix} \cdot \begin{bmatrix} \begin{bmatrix} c_K \\ s_K \end{bmatrix} \otimes \ldots \otimes \begin{bmatrix} c_1 \\ s_1 \end{bmatrix} \otimes \begin{bmatrix} c_0 \\ s_0 \end{bmatrix} \end{bmatrix}$$

The 2^K dimensional complex vector on the left side of the equation is proportional to the vector $\hat{T}_c(K)$ comprising the desired edited spectra

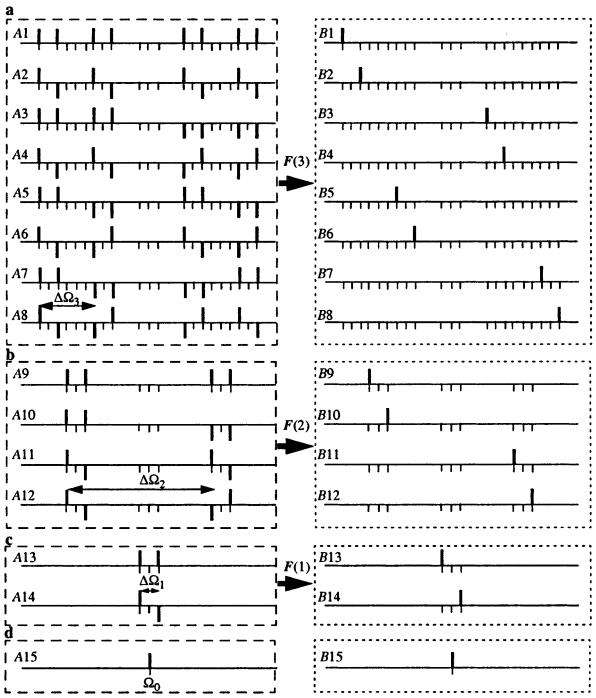

Figure 2. Stick diagram exemplifying the formation of chemical shift multiplets (on the left) for $K = 3$ and phase-sensitively edited multiplet components (on the right) in the frequency domain. (a) Basic spectra yielding the following linear combinations: $B1[\Omega_0 + \Omega_1 + \Omega_2 + \Omega_3] = A1 + A2 + A3 + A4 + A5 + A6 + A7 + A8$; $B2[\Omega_0 - \Omega_1 + \Omega_2 + \Omega_3] = A1 - A2 + A3 - A4 + A5 - A6 + A7 - A8$; $B3[\Omega_0 + \Omega_1 - \Omega_2 + \Omega_3] = A1 + A2 - A3 - A4 + A5 + A6 - A7 - A8$; $B4[\Omega_0 - \Omega_1 - \Omega_2 + \Omega_3] = A1 - A2 - A3 + A4 + A5 - A6 - A7 + A8$; $B5[\Omega_0 + \Omega_1 + \Omega_2 - \Omega_3] = A1 + A2 + A3 + A4 - A5 - A6 - A7 - A8$; $B6[\Omega_0 - \Omega_1 + \Omega_2 - \Omega_3] = A1 - A2 + A3 - A4 - A5 + A6 - A7 + A8$; $B7[\Omega_0 + \Omega_1 - \Omega_2 - \Omega_3] = A1 + A2 - A3 - A4 - A5 - A6 + A7 + A8$; $B8[\Omega_0 - \Omega_1 - \Omega_2 - \Omega_3] = A1 - A2 - A3 + A4 - A5 + A6 + A7 - A8$. (b) First-order central peak spectra: $B9[\Omega_0 + \Omega_1 + \Omega_2] = A9 + A10 + A11 + A12$; $B10[\Omega_0 - \Omega_1 + \Omega_2] = A9 - A10 + A11 - A12$; $B11[\Omega_0 + \Omega_1 - \Omega_2] = A9 + A10 - A11 - A12$; $B12[\Omega_0 - \Omega_1 - \Omega_2] = A9 - A10 - A11 + A12$. (c) Second-order central peak spectra: $B13[\Omega_0 + \Omega_1] = A13 + A14$; $B14[\Omega_0 - \Omega_1] = A13 - A14$. (d) Third-order central peak spectra: $B15 = A15$. For the calculation of the matrixes $F(K)$, see the Supporting Information, and for a definition of "basic" and "central peak" spectra, see the Theory section. To facilitate the comparison of the left and the right section, the positions of multiplet components are indicated with thin lines.

with the individual components of the chemical shift multiplets; that is, we have that

$$\hat{T}_c(K) \sim \begin{bmatrix} e^{i_K} \\ e^{-i_K} \end{bmatrix} \otimes \ldots \otimes \begin{bmatrix} e^{i_1} \\ e^{-i_1} \end{bmatrix} \otimes e^{i_0}$$

The 2^{K+1} dimensional real vector of the 2^{K+1} trigonometric modulations on the right side of the equation is proportional to the vector containing the spectra with the chemical shift multiplets in the real, *Sjr*, and imaginary parts, *Sji*, of the 2^K N_tD spectra ($j = 1 \ldots 2^K$). Hence, with $\hat{S}(K) = [S_{1r}\, S_{1i}\, S_{2r}\, S_{2i} \ldots S_{2^Kr}\, S_{2^Ki}]^T$, we have that

$$\hat{S}(K) \sim \begin{bmatrix} c_K \\ s_K \end{bmatrix} \otimes \ldots \otimes \begin{bmatrix} c_1 \\ s_1 \end{bmatrix} \otimes \begin{bmatrix} c_0 \\ s_0 \end{bmatrix}$$

For the $2^K \times 2^{K+1}$ complex G-matrix, which transforms $\hat{S}(K)$ into $\hat{T}(K)$ according to

$$\hat{T}_C(K) = \hat{G}_C(K) \cdot \hat{S}(K) \qquad (1)$$

one then obtains

$$\hat{G}_c(K) = \left[\begin{bmatrix} 1 & i \\ 1 & -i \end{bmatrix} \otimes \ldots \otimes \begin{bmatrix} 1 & i \\ 1 & -i \end{bmatrix} \otimes \begin{bmatrix} 1 & i \end{bmatrix} \right]$$

Alternatively, the multiplet components may be edited in the frequency domain (Figure 2). The spectra of $\hat{S}(K)$ are Fourier transformed, and a zero-order phase correction of $n \cdot 90°$ is applied, depending on the number n of chemical shift sine modulations (see the Supporting Information). The resulting real parts contain purely absorptive chemical shift multiplets and form the 2^K dimensional real vector $\hat{A}(K)$. Their linear combination yields the edited spectra contained in the 2^K dimensional real vector $\hat{B}(K)$ according to

$$\hat{B}(K) = \hat{F}(K) \cdot \hat{A}(K) \qquad (2)$$

Hence, $\hat{B}(K)$ represents spectra which contain the edited 2^K individual multiplet components at $\Omega_0 \pm \Omega_1 \pm \ldots \pm \Omega_K$ encoding the desired $K + 1$ chemical shifts. $\hat{F}(K)$ can be readily obtained from $\hat{F}(K-1)$ by tensor product formation using the relation $\hat{F}(K) = \hat{F}(K-1) \otimes \hat{F}(1)$, with

$$\hat{F}(1) = \begin{bmatrix} 1 & 1 \\ 1 & -1 \end{bmatrix}$$

(for details and the relation between F and the G-matrix, see the Supporting Information).

The 2^K spectra of $\hat{T}_c(K)$ and $\hat{B}(K)$ shall be designated "basic spectra". Additional information is required to unambiguously derive all shift correlations of the parent ND experiment (which resolves degeneracy in up to $N-1$ dimensions) if two multiplets exhibit degenerate chemical shifts in all of the *conventionally* sampled $N_t - 1$ dimensions. The acquisition of peaks defining the centers of the chemical shift splittings ("central peaks") at the frequencies $\Omega_0 \pm \Omega_1 \pm \ldots \pm \Omega_{K-1}$, $\Omega_0 \pm \Omega_1 \pm \ldots \pm \Omega_{K-2}$, . . ., $\Omega_0 \pm \Omega_1$, and Ω_0 is then needed for identifying the components forming a given multiplet (Figure 3a). Such "central peak acquisition" has previously been introduced in the framework of the reduced-dimensionality NMR approach[4,6] and is generalized here for GFT NMR. The shift correlations of the ND spectrum can be obtained by "bottom-up" identification of the shift multiplets. This procedure essentially groups the peaks of the basic spectra into sets each belonging to one multiplet (Figure 3). Because the basic peaks of two spin systems can be grouped even if central peaks overlap (Figure 3b), this approach ensures that all correlations of the ND experiment are retained. GFT NMR (Figure 1) thus requires one to record a total of $p = \sum_{k=0}^{K} 2^k = 2^{K+1} - 1$ N_tD spectra, including 2^K basic spectra and $2^K - 1$ central peak spectra. The p data sets constitute an "(N,N_t)D GFT NMR experiment", and we denote central peaks arising from the omission of m chemical shifts to be of mth order. For practical purposes, it is important to note that all components of a given multiplet have quite similar intensities because they are generated by multiple sine or cosine modulation of the transfer amplitude. Usually this does not hold for two peaks belonging to two different spin systems (Figure 3a) because the nuclear spin relaxation times determining the peak

(6) (a) Szyperski, T.; Wider, G.; Bushweller, J. H.; Wüthrich, K. *J. Biomol. NMR* **1993**, *3*, 127−132. (b) Szyperski, T.; Wider, G.; Bushweller, J. H.; Wüthrich, K. *J. Am. Chem. Soc.* **1993**, *115*, 9307−9308. (c) Szyperski, T.; Pellecchia, M.; Wüthrich, K. *J. Magn. Reson., Ser. B* **1994**, *105*, 188−191. (d) Brutscher, B.; Simorre, J. P.; Caffrey, M. S.; Marion, D. *J. Magn. Reson., Ser. B* **1994**, *105*, 77−82. (e) Szyperski, T.; Braun, D.; Fernández, C.; Bartels, C.; Wüthrich, K. *J. Magn. Reson., Ser. B* **1995**, *108*, 197−203. (f) Brutscher, B.; Morelle, N.; Cordier, F.; Marion, D. *J. Magn. Reson., Ser. B* **1995**, *109*, 238−242. (g) Szyperski, T.; Braun, D.; Banecki, B.; Wüthrich, K. *J. Am. Chem. Soc.* **1996**, *118*, 8146−8147. (h) Bracken, C.; Palmer, A. G.; Cavanagh, J. *J. Biomol. NMR* **1997**, *9*, 94−100. (i) Szyperski, T.; Banecki, B.; Braun, D.; Glaser, R. W. *J. Biomol. NMR* **1998**, *11*, 387−405. (j) Astrof, N. S.; Lyon, C. E.; Griffin, R. G. *J. Magn. Reson.* **2001**, *152*, 303−307. (k) Xia, Y.; Arrowsmith, C.; Szyperski, T. *J. Biomol. NMR* **2002**, *24*, 41−50.

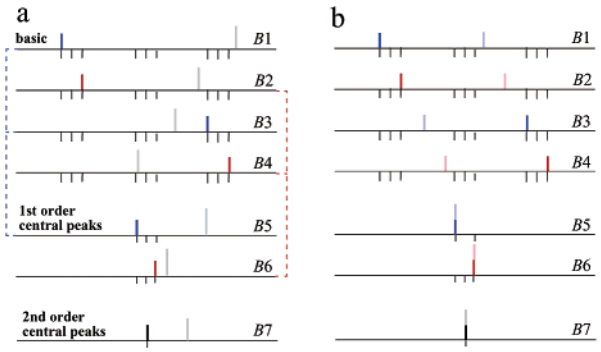

Figure 3. "Bottom-up" identification of the peaks forming a chemical shift multiplet in GFT NMR provided that three indirect dimensions of a FT NMR experiment are jointly sampled (Figure 1; $K = 2$). (a) Two spin systems exhibiting degenerate chemical shifts in all other conventionally sampled $N_t - 1$ dimensions give rise to basic, first-order central, and second-order central peaks shown in bold colors (spin system 1) and gray (spin system 2), respectively. Knowledge of the position of the second-order central peak of spin system 1 allows for identification of the corresponding first-order central peaks of spin system 1. In turn, their knowledge allows unambiguous identification of the corresponding peaks of spin system 1 in the basic spectra. As indicated by the colored dashed lines, the peaks in *B*1 and *B*3 are centered around the peak in *B*5 (shown in blue), while the peaks in *B*2 and *B*4 are centered around the peak in *B*5 (shown in red). This strategy can readily be extended for $K > 2$. In practice, the identification of components belonging to a given shift of multiplets is greatly facilitated by inspection of peak intensities: the components forming a given multiplet are expected to exhibit (nearly) the same intensity. To illustrate this point, the resonance lines of spin system 2 were assumed to be more intense than those of spin system 1 (see text). (b) In addition to chemical shift degeneracy in the conventionally sampled $N_t - 1$ dimensions, the central peaks of spin system 1 (as described in a) and those of spin system 3 (peaks shown in gray or faint color) overlap. In this case, the two spin systems exhibit degenerate chemical shifts in all but one dimension of an *N*D FT NMR spectrum. In (N,N_t)D GFT NMR, the bottom-up identification of multiplet components resolves and groups the signals of the two spin systems in the basic spectra, thus yielding the equivalent of the *N*D chemical shift correlation.

intensities vary from spin system to spin system. Hence, inspection of peak intensities greatly facilitates the grouping of the peaks.

The joint sampling of several indirect dimensions reduces the minimal measurement time, T_m, of an (N,N_t)D GFT NMR experiment when compared with the parent *N*D FT experiment. The $K + 1$ dimensions of an FT NMR spectrum exhibiting the spectral widths SW_0, SW_1, . . . SW_K are sampled with n_0, n_1, . . . n_K complex points and yield maximal evolution times of $t_{0,max}$, $t_{1,max}$, . . . $t_{K,max}$. In the (N,N_t)D GFT NMR experiment, the same maximal evolution times of the parent *N*D experiment can be realized by appropriate scaling of increments.[6a,c] The acquisition of both cosine and sine modulated spectra for all jointly sampled chemical shifts (eq 1) corresponds to their phase-sensitive acquisition[6f] and allows one to place the rf carrier positions in the center of the spectral ranges. Hence, the spectral width required for combined sampling is given by $SW = \sum_{j=0}^{K} \kappa_j \cdot SW_j$, where κ_j represents the factor to scale[6a,c] the sampling increments of the *j*th dimension to adjust maximal evolution times. If the same maximal evolution time is chosen for all dimensions and assuming, for simplicity, that delayed acquisition starts at $1/SW_j$, $n = \sum_{j=0}^{K} n_j$ complex points are required to sample the resulting single dimension [if acquisition starts at $t = 0$, one obtains that $n = (\sum_{j=0}^{K} n_j) - K$]. The ratio ϵ of the minimal measurement time of an FT NMR experiment, T_m(FT), and the corresponding GFT NMR experiment, T_m(GFT), is then given by the number of FIDs that are required to sample the $K + 1$ FT NMR dimensions divided by p times the number of FIDs required to sample the resulting single dimension:

$$\epsilon = \frac{T_m(\mathrm{FT})}{T_m(\mathrm{GFT})} = (2^K/(2^{K+1} - 1)) \cdot (\prod_{j=0}^{K} n_j)/(\sum_{j=0}^{K} n_j) \qquad (3)$$

This ratio scales with the product of the number of points over the corresponding sum and thus predicts large reductions in T_m (Table S1; different ways to implement central peak acquisition as well as the impact of a particular implementation on ϵ are described in the Supporting Information).[7] The S/N of each of the 2^K components in the basic spectra is reduced by $(1/\sqrt{2})^K$ as compared to the single peak in FT NMR. This is because each chemical shift splitting reduces the S/N by a factor of 2 relative to the FT NMR spectrum, while a factor of $\sqrt{2}$ is gained because frequency discrimination is not associated with a FT (see Figure 2: both cosine and sine modulated parts contribute equally to the signal intensity in the edited spectra).[8]

NMR Spectroscopy. For the 76-residue protein ubiquitin, nearly all signals of 2D [^{15}N,^{1}H]-HSQC[2] are resolved so that $N_t = 2$ is an obvious choice. As an application, we thus recorded a (5,2)D GFT NMR HACACONHN experiment ($K = 3$) within 138 min on a Varian Inova 600 spectrometer using the HACACONHN rf pulse sequence shown in Figure 4. This experiment correlates the polypeptide backbone ^{1}H$^{\alpha}$, ^{13}C$^{\alpha}$, and ^{13}C′ chemical shifts of residue i with the backbone amide ^{15}N and ^{1}H^{N} chemical shifts of residue $i + 1$. The underlined letters denote that $\Omega_3(^{1}H^{\alpha})$, $\Omega_2(^{13}C^{\alpha})$, $\Omega_1(^{13}C')$, and $\Omega_o(^{15}N)$ are measured in a single dimension. A 2 mM solution of ^{15}N/^{13}C doubly labeled ubiquitin in 90% H_2O/10% D_2O (50 mM K−PO_4; pH = 5.8) was used at T = 25 °C.

With the HACACONHN rf pulse scheme of Figure 4, 16 individual data sets $R1-R16$ (to provide basic and first-order central peaks) were acquired in 6.9 min each, with $SW_1(^{15}N/^{13}C'/^{13}C^{\alpha}/^{1}H^{\alpha}) = 8000$ Hz and $53(t_1)$*$512(t_2)$ complex points [$t_{1,max}(^{15}N/^{13}C'/^{13}C^{\alpha}/^{1}H^{\alpha}) = 6.5$ ms; $t_{2,max}(^{1}H^{N}) = 73.2$ ms], yielding after data processing (see the Supporting Information) the 12 planes $B1-B12$ containing basic and first-order central peaks. The phases of the 90° rf pulses generating transverse ^{15}N, ^{13}C′, ^{13}C$^{\alpha}$, and ^{1}H$^{\alpha}$ magnetization for frequency labeling are ϕ_0, ϕ_1, ϕ_2, and ϕ_3, respectively (Figure 4). ϕ_0 is altered between 0° and 90° for phase-sensitive acquisition[2] of $\Omega_o(^{15}N)$ along t_1. The three phases ϕ_1, ϕ_2, and ϕ_3 are independently altered between 0° and 90° for frequency discrimination of $\Omega_1(^{13}C')$, $\Omega_2(^{13}C^{\alpha})$, and $\Omega_3(^{1}H^{\alpha})$ in the first eight data sets $R1-R8$. For first-order central peak detection using ^{13}C steady-state magnetization,[6g,i] the eight measurements are repeated with the first 90° pulse on ^{1}H$^{\alpha}$ being shifted by 180°. This yields the following phase cycle for the 16 data sets $R1-R16$: $\phi_1 = 8(x, y)$; $\phi_2 = 4(2x, 2y)$; $\phi_3 = 4x, 4y, 4(-x), 4(-y)$ with the receiver phase being unchanged. A reduced dimensionality[4,6b] 2D HNNCO spectrum (second-order central peaks) derived from a HNNCO scheme[3] was acquired in 13.8 min with $SW(^{15}N/^{13}C') = 8000$ Hz and $128(t_1)$*$512(t_2)$ complex points [$t_{1,max}(^{15}N/^{13}C') = 15.9$ ms; $t_{2,max}(^{1}H^{N}) = 73.2$ ms], yielding data sets *R*17 and *R*18 (*B*13 and *B*14 after data processing; see the Supporting Information) with phase $\phi_3 = (x, y)$. A 2D [^{15}N,^{1}H]-HSQC spectrum[2] (third-order central peaks) was acquired in 13.8 min with $SW(^{15}N) = 8000$ Hz and $256(t_1)$*$512(t_2)$ complex points [$t_{1,max}(^{15}N) = 26$ ms; $t_{2,max}(^{1}H^{N}) = 73.2$ ms], yielding the data set *R*19 (*B*15 after data processing; see the Supporting Information). For larger systems requiring longer measurements, it might be advisable to derive second- and third-order central peaks from ^{13}C′ and ^{15}N steady-state magnetization, respectively. The total measurement time of the 19 data sets was 138 min. To obtain pure phases, zero first-order phase corrections must

(7) The GFT NMR scheme can be generalized by its *M*-fold application. Because this would involve *M* different *G*-matrixes, such an experiment could be designated a G^{M}FT NMR experiment. For example, two groups of dimensions can be identified with each group being combined to a single dimension. First an (N,N')D experiment is devised in which dimensions 1,2 . . . i are jointly sampled. Subsequently, the dimensionality of this experiment is reduced to an (N,N_t) experiment by jointly sampling dimensions $i + 1$, $i + 2$,. . . $K + 2$. For *M* projection steps, each invoking different sets of dimensions combined to a single one, the total reduction in minimal measurement time is then given by $\epsilon^{tot} = \prod_{j=1}^{M} \epsilon_j$, where ϵ_j is the reduction due to the *j*th projection (eq 3).

(8) The S/N ratio of FT NMR can be recovered by symmetrization about central peaks as described for reduced-dimensionality NMR[6e] using the "bottom-up" strategy employed for identification of shift multiplets (Figure 3). Note that a reduced sensitivity is not relevant in the sampling limited regime.

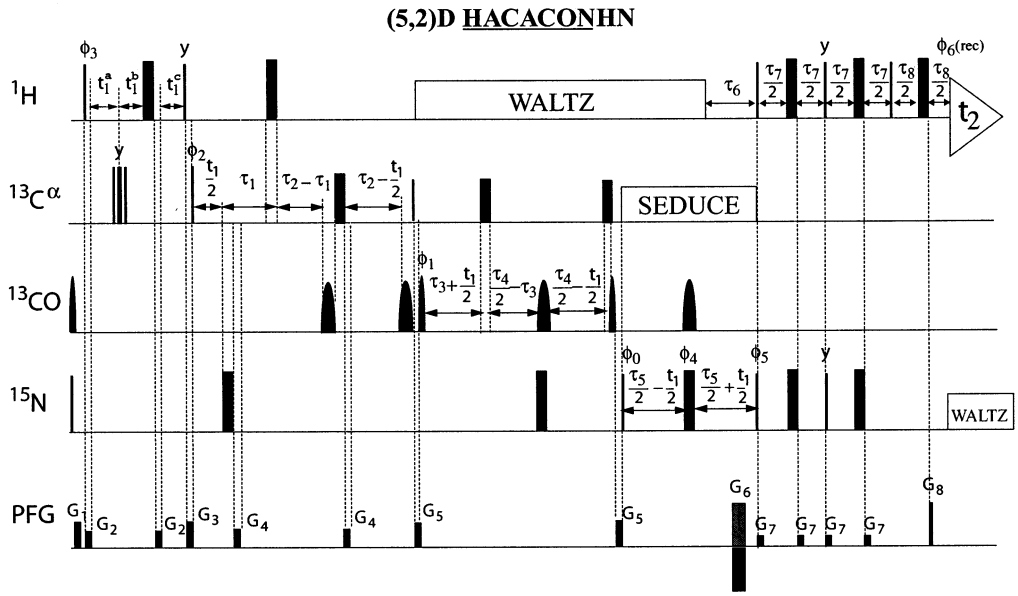

Figure 4. Rf pulse sequence used to record the (5,2)D HACACONHN GFT NMR experiment. Rectangular 90° and 180° pulses are indicated by thin and thick vertical bars, respectively, and phases are indicated above the pulses. Where no rf phase is marked, the pulse is applied along *x*. The high power 90° pulse lengths were 5.6 μs for ^{1}H and 15.3 μs for ^{13}C, and 39 μs for ^{15}N. Pulses on ^{13}C prior to t_1(^{13}C) are applied at high power, and ^{13}C decoupling during t_1(^{1}H) is achieved using a ($90_x-180_y-90_x$) composite pulse.[2] Subsequently, the 90° and 180° pulse lengths of ^{13}C$^\alpha$ are adjusted to 51.6 and 46 μs, respectively, to minimize perturbation of the ^{13}CO spins.[3] The width of the 90° pulses applied to ^{13}CO pulse is 51.6 μs, and the corresponding 180° pulses are applied with same power. A SEDUCE[3] 180° pulse with a length of 252 μs is used to decouple ^{13}CO during t_1. WALTZ16[2] is employed to decouple ^{1}H (rf field strength = 9.2 kHz) during the heteronuclear magnetization transfers as well as to decouple ^{15}N (rf = 1.78 kHz) during acquisition. The SEDUCE sequence (rf = 1.0 kHz) is used for decoupling of ^{13}C$^\alpha$ during the ^{15}N chemical shift evolution period. The ^{1}H rf carrier is placed at 4.78 ppm. The ^{13}C$^\alpha$, ^{13}C′, and ^{15}N rf carriers are set to 56.3, 174.3, and 119.3 ppm, respectively. The duration and strengths of the pulsed z-field gradients (PFGs) are G1 (1 ms, 24 G/cm); G2 (100 μs, 16 G/cm); G3 (1 ms, 24 G/cm); G4 (250 μs, 30 G/cm); G5 (1.5 ms, 20 G/cm); G6 (1.25 ms, 30 G/cm); G7 (500 μs, 8 G/cm); G8 (125 μs, 29.5 G/cm). All PFG pulses are of rectangular shape. The delays are τ_1 = 1.6 ms, τ_2 = 3.6 ms, τ_3 = 4.4 ms, $\tau_4 = \tau_5$ = 24.8 ms, τ_6 = 5.5 ms, τ_7 = 4.6 ms, τ_8 = 1 ms. ^{1}H-frequency labeling is achieved in a semiconstant-time fashion with t_1^a (0) = 1.79 ms, t_1^b (0) = 1 μs, t_1^c (0) = 1.791 ms, Δt_1^a = 62.5 μs, Δt_1^b = 32.9 μs, $\Delta t_1^c = -29.6$ μs. Hence, the fractional increase of the semiconstant-time period with t_1 is equal to $\lambda = 1 + \Delta t_1^c/\Delta t_1^a = 0.53$. Phase cycling: $\phi_0 = x$; $\phi_1 = x, -x$; $\phi_2 = x, x, -x, -x$; $\phi_3 = x$; $\phi_4 = 4x, 4(-x)$; ϕ_6(receiver) = $2(x, -x, -x, x)$. The sensitivity enhancement scheme of Kay et al.[21] is employed; that is, the sign of G6 is inverted in concert with a 180° shift of ϕ_5. Quadrature detection is accomplished by altering the phase ϕ_0 according to States-TPPI.[3] For the setting of the phases ϕ_0, ϕ_1, ϕ_2, and ϕ_3, see the NMR Spectroscopy section.

be ensured along ω_1 by, for example, starting sampling at $t_1 = 0$ for all of the combined chemical shift evolution periods. Editing of chemical shift multiplets in the time domain is advantageous, because the extension of the time domain data by linear prediction[2] (from 53 to 106 complex points for data sets $T1-T12$ and from 128 to 192 for data sets T13 and T14) profits from both maximizing the signal-to-noise of the time domain data and reducing the number of chemical shifts ("oscillators") to be predicted. The digital resolution after FT and zero-filling was 7.8 Hz/point along ω_1 and 6.9 Hz/point along ω_2.

A 5D FT HACACONHN spectrum acquired with the same maximal evolution times as the basic spectra of (5,2)D HACACONHN would require sampling of $10(t_1)*11(t_2)*22(t_3)*13(t_4)*512(t_5)$ complex points [i.e., $n = (\sum_{j=0}^{K} n_j) - K$] with spectral widths of $SW_1(^{15}N)$ = 1440 Hz, $SW_2(^{13}C') = 1500$ Hz, $SW_3(^{13}C^\alpha) = 3260$ Hz, and $SW_4(^1H^\alpha) = 1800$ Hz (i.e., $SW = \sum_{j=0}^{K} SW_j$) in 5.83 days of spectrometer time. For comparison of digital resolution in FT and GFT NMR, 2D [ω_1,ω_5]-, [ω_2,ω_5]-, [ω_3,ω_5]-, and [ω_4,ω_5]-planes of the 5D FT HACACONHN experiment were recorded in 1.3, 1.4, 2.9, and 1.7 min, respectively. For line width comparisons with (5,2)D GFT HACACONHN, the same planes were also acquired with spectral widths of SW = 8000 Hz in the indirect dimension.

Peak Assignment and Calculation of Chemical Shifts. The chemical shift multiplets encoded in the edited spectra $B1-B15$ of (5,2)D HACACONHN were identified starting from an assigned [^{15}N,^{1}H]-HSQC peak list in the "bottom-up" manner described in Figure 3. The resulting peak lists of $B1-B15$ were then used as input for a least-squares fitting routine[9,10] solving an overdetermined system of 15 equations resulting from the ω_1-frequencies of the 15 peaks. This yielded the correlations involving $\Omega(^1H_i^\alpha)$, $\Omega(^{13}C_i^\alpha)$, $\Omega(^{13}C_i')$, $\Omega(^{15}N_{i+1})$, and $\Omega(^1H_{i+1}^N)$ (Table S2). A Monte Carlo simulation of error propagation (see legend of Figure 8 for details) served to provide an estimate for the standard deviations for the chemical shift measurements based on the measurements of line widths.

Results and Discussion

As an application, we acquired a (5,2)D HACACONHN GFT NMR experiment for the 8.6 kDa protein ubiquitin. Figure 5 shows the chemical shift multiplets as well as the resulting edited multiplet components, and Figure 6 shows all 15 planes constituting the (5,2)D HACACONHN experiment. The bottom-up identification (Figure 3) of components forming a given shift multiplet allows one to retain the 5D correlations of the parent experiment. Peak detection was nearly complete so that a total of 67 chemical shift 5-tuples as well as 3 shift 6-tuples for glycines with nondegenerate $^1H^\alpha$ shifts (Table S2) were obtained. The S/N ratios obtained in the GFT NMR experiment[11] demonstrate adequate adjustment of the measurement time to sensitivity requirements while the desired 5D chemical shift correlations were registered. The ratios also show that conven-

(9) Eadie, W. T.; Drijard, D.; James, F. E.; Roos, M.; Sadoulet, B. *Statistical Methods in Experimental Physics*; North-Holland: New York, 1982.

(10) Lau, H. T. *A Numerical Library in C for Scientists and Engineers*; CRC Press: Boca Raton, FL, 1995.

(11) The S/N ratios were between 6.4 and 12.0 in the basic spectra (Figure 6a), and between 5.6 and 10.4 for first-order peaks (Figure 6b), between 9.8 and 24.0 for second-order peaks (Figure 6c), and between 44.0 and 108.0 for third-order central peaks (Figure 6d).

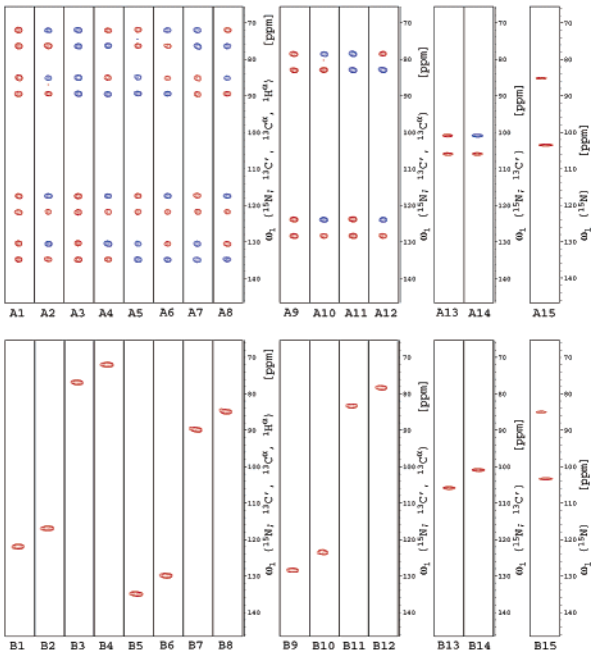

Figure 5. $\omega_1[(^{15}N;^{13}C',^{13}C^{\alpha},^{1}H^{\alpha})$, $\omega_2(^{1}H^{N})]$-, $[\omega_1(^{15}N;^{13}C',^{13}C^{\alpha})$, $\omega_2(^{1}H^{N})]$-, $[\omega_1(^{15}N;^{13}C')$, $\omega_2(^{1}H^{N})]$-, and $[\omega_1(^{15}N)$, $\omega_2(^{1}H^{N})]$-strips taken from the (5,2)D HACACONHN GFT NMR experiment (see Figure 6). The signals were detected on the amide proton chemical shift of Ser 20. Positive and negative contour levels are shown in red and blue, respectively. (a) Spectra *A*1−*A*15 containing the chemical shift multiplets. (b) Spectra *B*1−*B*15 containing the individual edited chemical shift multiplet components. Note that when compared with Figure 2, the order of the chemical shift multiplets appears to have changed. However, this is because $\omega_1(^{1}H^{\alpha}) < 0$ ppm (i.e., upfield relative to the carrier position) for Ser 20, and $\omega_1(^{13}C')$, $\omega_1(^{13}C^{\alpha})$, and $\omega_1(^{15}N) > 0$ ppm (i.e, downfield relative to the respective carrier position). For simplicity, Figure 2 was designed with the assumption that all resonances are located downfield to the respective carrier positions. The signals located at higher field in *A*15 and *B*15 arise from a side chain moiety and thus have no corresponding peaks in the other spectra (see also Figure 6d). To facilitate the comparison of (a) and (b), the positions of multiplet components are indicated with thin lines.

tional 4D or 5D HACACONHN experiments would have to be acquired in the sampling limited data collection regime because their minimal measurements are on the order of several days.

Because equivalent chemical shift correlations are provided by (5,2)D HACACONHN GFT and 5D HACACONHN FT NMR, these two experiments can be compared in terms of minimal measurement times and data sizes. An evident advantage of the GFT NMR experiment is the large reduction in T_m. Equation 3 predicts reductions in measurement times of about an order of magnitude for each dimension included into the joint sampling scheme (Table S1). In fact, the minimal measurement times with a single scan per FID each second (and the same t_{max} for all chemical shift evolution periods as chosen for basic and first-order central peak acquisition) are 33.5 min and 5.83 days for (5,2)D HACACONHN GFT NMR (Figure 6) and 5D HACACONHN FT NMR, revealing a 250-fold reduction in T_m for the GFT experiment (note that this value deviates from $\epsilon = 317$ obtained with eq 3 due to the particular choice to implement central peak acquisition; see Theory section and Supporting Information). Concomitantly, the data size is largely reduced when transformed data sets with equal digital resolution are compared (Figure 7).

To assess the precision of the chemical shift measurements, the resonance line widths need to be considered.[2] In general, the joint sampling of $K + 1$ *nonconstant-time* chemical shift evolution periods yields transfer amplitudes attenuated by $\exp(-\sum_{j=0}^{K} R_{2,j} \cdot t)$, where $R_{2,j}$ represents the transverse relaxation rate constant of the *j*th dimension. However, higher-dimensional heteronuclear FT NMR shift correlation spectra are quite often recorded with frequency labeling being accomplished in a constant-time manner[3] and/or with $t_{j,max} \ll 1/R_{2,j}$ for all *j*. As for the present implementation of (5,2)D HACACONHN, the line width is then determined[11] by the t_{max} values but is not dependent on $R_{2,j}$. Assuming for simplicity that all $t_{j,max}$ are identical, the 2^K lines of the chemical shift multiplets exhibit the same width as the corresponding single peak in *N*D FT NMR along each of the dimensions. Hence, peaks are not broadened in constant-time GFT NMR spectra with increasing *K*.[12] This is neatly confirmed when comparing ω_1 cross sections from (5,2)D HACACONHN with those taken from 2D HACACONHN spectra (Figure 7a,b).

The fact that the individual multiplet components possess the same line widths as the corresponding signals in the parent FT NMR experiment (Figure 7a,b) has a profound impact on the precision of the chemical shift measurement in constant-time GFT NMR experiments such as (5,2)D HACACONHN. To relate line widths to errors of measurement, we adopted a conservative statistical model in which (i) the error for the identification of peak positions is associated with a Gaussian distribution, and (ii) the Lorenzian line width, $\Delta\nu_{1/2}$, represents the corresponding 99.5% confidence interval (i.e., $\Delta\nu_{1/2} = 6\sigma$). σ(basic), σ(first), σ(second), and σ(third) are the standard deviations for shift measurements in basic, first-order, second-order, and third-order central peak spectra, respectively. Considering (i) that lines do not broaden with increasing *K* (Figure 7a,b) and (ii) the different maximal evolution times (see NMR Spectroscopy section), one has that $\sigma(\text{basic}) = \sigma(\text{first}) = \sigma^{FT}(^{13}C^{\alpha}) = \sigma^{FT}(^{1}H^{\alpha})$, $\sigma(\text{second}) = \sigma^{FT}(^{13}C')$, and $\sigma(\text{third}) = \sigma^{FT}(^{15}N)$. $\sigma^{FT}(X)$ represents the standard deviation for the chemical shift measurement of nucleus X ($^{1}H^{\alpha}$, $^{13}C^{\alpha}$, $^{13}C'$, ^{15}N) in conventional FT NMR spectra acquired with corresponding t_{max}. We performed Monte Carlo simulations to calculate the standard deviations $\sigma(^{13}C^{\alpha})$, $\sigma(^{1}H^{\alpha})$, $\sigma(^{13}C')$, and $\sigma(^{15}N)$ in (5,2)D HACACONHN GFT NMR for various selections of subspectra (Figures 8, S1). If a minimal number of four basic spectra is selected to calculate $\Omega_3(^{1}H^{\alpha})$, $\Omega_2(^{13}C^{\alpha})$, $\Omega_1(^{13}C')$, and $\Omega_o(^{15}N)$, the precision depends on which four are selected (see Figure S1 and its legend for details). In the two most favorable cases, the standard deviations in the constant-time GFT NMR experiment are reduced by a factor of $2 = \sqrt{4}$, that is, $\sigma(X) = {}^{1}/_{2} \cdot \sigma^{FT}(^{1}H^{\alpha}) = {}^{1}/_{2} \cdot \sigma^{FT}(^{13}C^{\alpha}) = {}^{1}/_{2} \cdot \sigma(\text{basic})$. If the eight basic spectra are selected, the standard deviation is reduced by an additional factor of $\sqrt{2}$, yielding $\sigma(X) = {}^{1}/_{\sqrt{8}} \cdot \sigma(\text{basic})$. Similarly, $\sigma(X) = {}^{1}/_{\sqrt{12}} \cdot \sigma(\text{basic})$ if both the eight basic and the four first-order central peak spectra are chosen. The exact match between reductions by a factor of $\sqrt{n}$, where *n* represents the number of spectra, and the reductions obtained from the simulations (see legends of Figures 8, S1 for details) reflects

(12) The width at half-height of the frequency domain sinc centre lobe resulting from truncation in the time domain at t_{max} is given[2] by $0.604/t_{max}$. In the current implementation of (5,2)D HACACONHN (Figure 4), all indirect evolution periods except for $\Omega(^{1}H^{\alpha})$ are constant-time periods. The evolution of $\Omega(^{1}H^{\alpha})$ is implemented in a semiconstant-time manner,[3] so that signal losses due to transverse relaxation of $^{1}H^{\alpha}$ are negligible for 8.6 kDa ubiquitin at short t_{max} values around 6.5 ms. For larger systems with short $T_2(^{1}H^{\alpha})$, however, the semiconstant-time frequency labeling may lead to a detectable increase of ω_1-line widths in the basic when compared to central peak spectra.

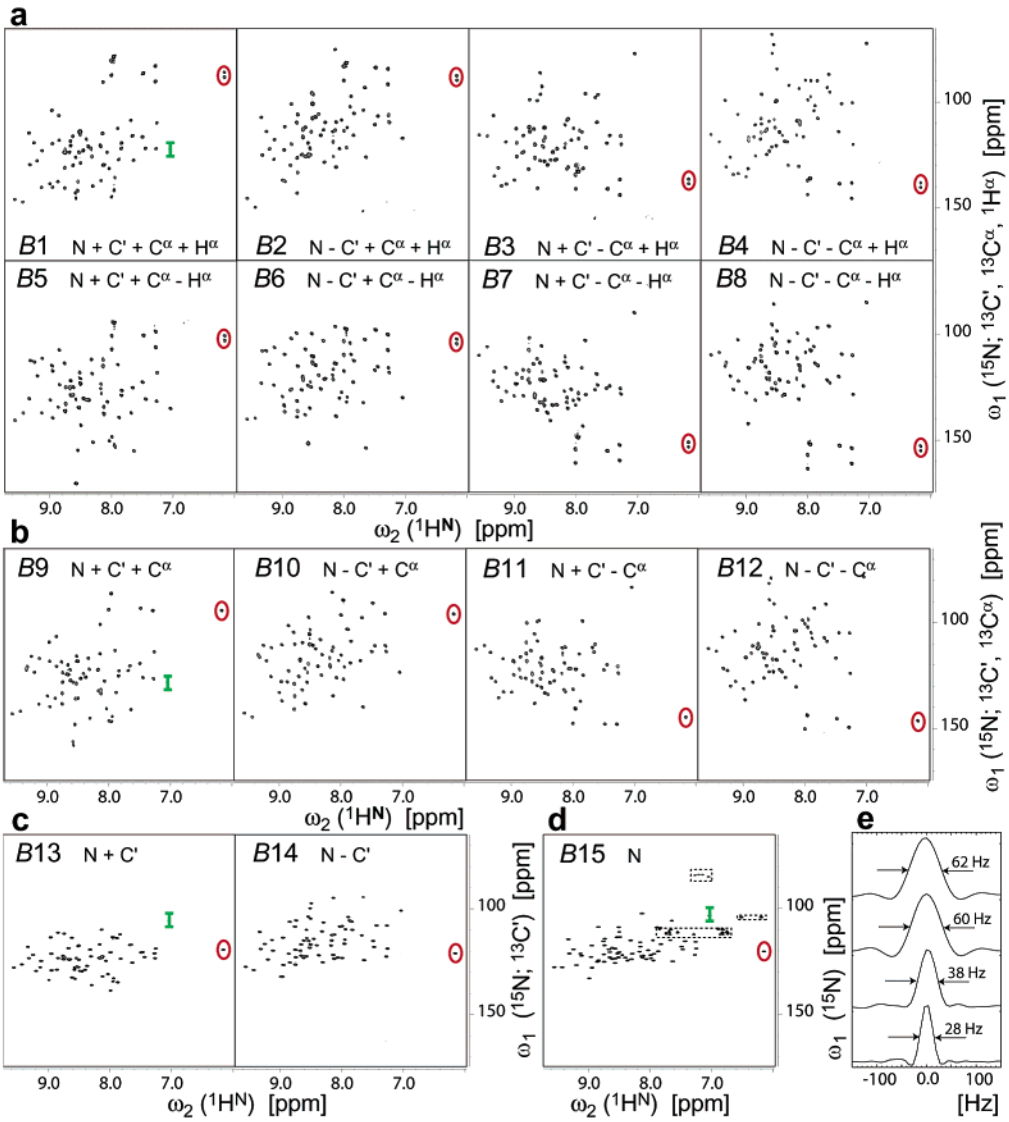

Figure 6. The 15 2D planes constituting the (5,2)D HACACONHN GFT NMR experiment ($K = 3$) recorded for the 8.6 kDa protein ubiquitin. The linear combination of chemical shifts detected in a given plane is indicated. (a) The basic spectra $B1-B8$. (b) First-order central peak spectra $B9-B12$. (c) Second-order central peak spectra $B13$ and $B14$. (d) Third-order central peak spectrum $B15$. Signals arising from side chain moieties are in dashed boxes. (e) Cross sections taken along $\omega_1(^{15}N;^{13}C',^{13}C^{\alpha},^{1}H^{\alpha})$ at the peak of Ser 20 in $B1$ (at the top), along $\omega_1(^{15}N;^{13}C',^{13}C^{\alpha})$ in $B9$ (second from top), along $\omega_1(^{15}N;^{13}C')$ in $B13$ (third from top), and along $\omega_1(^{15}N)$ in $B15$ (at the bottom). The sections are indicated in green in the corresponding panel. Comparison of sections from $B1$ and $B9$ shows that signals do not broaden with increasing K (Figure 7), while the smaller line widths observed in spectra $B13-B15$ result from longer t_{max} values (see NMR Spectroscopy section). The 15 signals detected on the backbone amide proton of Ile 36 are circled in red. Doublets are observed in $B1-B8$ because Gly 35 exhibits nondegenerate $^{1}H^{\alpha}$ chemical shifts, yielding the correlation of six shifts: $\delta(^{1}H^{\alpha 2}) = 4.135 \pm 0.006$ ppm, $\delta(^{1}H^{\alpha 1}) = 3.929 \pm 0.006$ ppm, $\delta(^{13}C^{\alpha}) = 46.10 \pm 0.019$ ppm, $\delta(^{13}C') = 173.911 \pm 0.017$ ppm for Gly 35, and $\delta(^{15}N) = 120.295 \pm 0.043$ ppm and $\delta(^{1}H^{N}) = 6.174 \pm 0.005$ ppm for Ile 36 (Table S2). The standard deviations of the indirectly detected chemical shifts were estimated from a Monte Carlo simulation (see legend of Figure 8). In accordance, the $\omega_2(^{1}H^{N})$ line width of the directly detected amide proton (20 Hz) was identified with $\pm 3\sigma$ (99.5% confidence interval) for locating the peak positions. Notably, phase-sensitive editing of the chemical shift multiplets yields increasing peak dispersion (and thus resolution) in each of the constituent spectra as compared to 2D [^{15}N,^{1}H]-HSQC (panel $B15$). Nearly the same number of peaks are detected in each of 15 spectra, while the spectral width increases from $SW_1(^{15}N) = 1440$ Hz in $B15$ to $SW_1(^{15}N/^{13}C'/^{13}C^{\alpha}/^{1}H^{\alpha}) = 8000$ Hz in $B1-B8$.

the well-known relation from statistics[9] stating that the standard deviation of an average arising from n multiple independent measurements is reduced by a factor of $\sqrt{n}$ (Figure 1). For the current implementation of (5,2)D HACACONHN, second- and third-order central peak spectra were acquired with longer maximal evolution times than the first-order central peak and basic spectra (Figure 6e; see NMR Spectroscopy section). Hence, $\sigma(^{13}C')$ and $\sigma(^{15}N)$ turn out to be somewhat smaller than $^{1}/_{\sqrt{14}} \cdot \sigma$(basic) and $^{1}/_{\sqrt{15}} \cdot \sigma$(basic), respectively, when 14 or all 15 spectra are considered (see legend of Figure S1 for details). When compared with σ(second) $= \sigma^{FT}(^{13}C')$ and σ(third) $= \sigma^{FT}(^{15}N)$, which reflect rather long maximal evolution times, the values of $\sigma(^{13}C')$ and $\sigma(^{15}N)$ are reduced by factors of 2.5 and 2.0, respectively. The Monte Carlo simulations are in neat agreement with analytical calculations of standard deviations using the Gaussian law of error propagation[9] (see legend of Figure S1) and are evidently a valuable tool to analyze the precision of shift measurements in more intricate future implementations of GFT NMR experiments.

Overall, the precision of the indirect shift measurements in the (5,2)D HACACONHN experiment [$\sigma(^{1}H^{\alpha}) = 3.7$ Hz, $\sigma(^{13}C^{\alpha}) = 2.9$ Hz, $\sigma(^{13}C') = 2.6$ Hz, $\sigma(^{15}N) = 2.4$ Hz] matches the one obtained in the direct dimension [$\sigma(^{1}H^{N}) = 3.3$ Hz]. Remarkably, one can anticipate for molecules tumbling slower

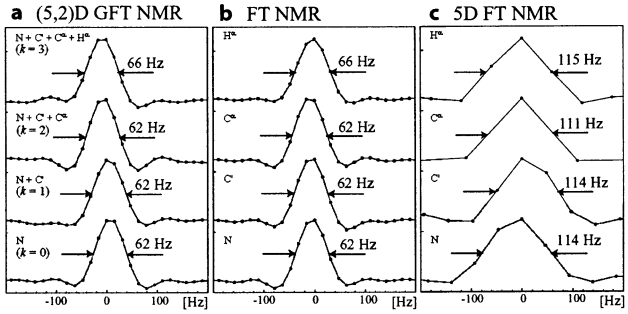

Figure 7. Comparison of line widths and digital resolution of peaks detected in GFT and FT NMR. (a) (5,2)D HACACONHN GFT NMR: cross sections taken along $\omega_1(^{15}N;^{13}C',^{13}C^{\alpha},^{1}H^{\alpha})$ at the peak of Ser 20 in spectrum *B*1 (at the top), along $\omega_1(^{15}N;^{13}C',^{13}C^{\alpha})$ in spectrum *B*9 (second from top), along $\omega_1(^{15}N;^{13}C')$ in spectrum *B*13 (third from top), and along $\omega_1(^{15}N)$ in spectrum *B*15 (at the bottom). The same t_{max} value was chosen for all spectra to demonstrate that resonances do not broaden when increasing *K* from 0 to 3 (see text). (b) HACACONHN FT NMR: $\omega_1(^1H^{\alpha})$, $\omega_1(^{13}C^{\alpha})$, $\omega_1(^{13}C')$, and $\omega_1(^{15}N)$ cross sections taken from 2D $[\omega_1,\omega_2(^1H^N)]$-planes obtained with the HACACONHN rf pulse scheme which were (i) recorded with the same t_{max} values and spectral widths and (ii) processed as the (5,2)D HACACONHN planes (Figure 6). Comparison of (a) and (b) shows that the line width registered in the GFT NMR experiment equals the line width in the FT NMR experiment. (c) The same cross sections as in (b) are shown except that the planes were recorded and processed as a conventional 5D NMR spectrum would be [same maximal evolution times as in the basic spectra, $10(t_1)*11(t_2)*22(t_3)*13(t_4)*512(t_5)$ complex points with spectral widths of $SW_1(^{15}N) = 1440$ Hz, $SW_2(^{13}C') = 1500$ Hz, $SW_3(^{13}C^{\alpha}) = 3260$ Hz, and $SW_4(^1H^{\alpha}) = 1800$ Hz and linear prediction to $20(t_1)*22(t_2)*32(t_3)*26(t_4)*512(t_5)$ complex points]. This would yield a frequency domain data set of $32(\omega_1)*32(\omega_2)*32(\omega_3)*32(\omega_4)*512(\omega_5)$ real points of 2.1 GB size as compared to 16.8 MB for (5,2)D HACACONHN. Comparison with (b) and (c) makes the relatively poor resolution obtainable in 5D FT NMR apparent. Note that linear prediction and zero filling to $96(\omega_1)*96(\omega_2)*256(\omega_3)*128(\omega_4)*512(\omega_5)$ real points, which would be the closest match to the digital resolution obtained in (5,2)D HACACONHN, would result in an unrealistically large data size of 618 GB.

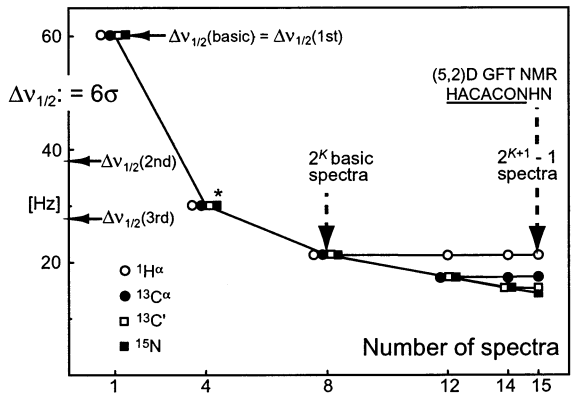

Figure 8. Monte Carlo simulations performed to assess the increased precision of chemical shift measurements in (5,2)D HACACONHN GFT NMR. Standard deviations for the chemical shift measurements are plotted versus the number of spectra selected from the 15 2D spectra constituting this experiment (Figure 6) to calculate the chemical shifts. $\sigma(^1H^{\alpha})$, $\sigma(^{13}C^{\alpha})$, $\sigma(^{13}C')$, and $\sigma(^{15}N)$ represent the deviations for $\Omega_3(^1H^{\alpha})$, $\Omega_2(^{13}C^{\alpha})$, $\Omega_1(^{13}C')$, and $\Omega_o(^{15}N)$ measurements, respectively. The following conservative statistical model is adopted. Line widths at half-height, $\Delta\nu_{1/2}$, were measured along ω_1 in (i) *B*1−*B*12 (basic spectra and first-order central peaks) providing $\Delta\nu_{1/2}(\text{basic}) = \Delta\nu_{1/2}(\text{first}) = 60.1$ Hz, (ii) *B*13 and *B*14 (second-order central peaks) providing $\Delta\nu_{1/2}(\text{second}) = 38.2$ Hz, and (iii) *B*15 (third-order central peaks) providing $\Delta\nu_{1/2}(\text{third}) = 28.1$ Hz [Figure 6e; these values are close to those expected[11] from the t_{max} values obtained after linear prediction]. It is then assumed that the error for the identification of peak positions is associated with a Gaussian distribution and that the Lorenzian line width, $\Delta\nu_{1/2}$, represents $\pm 3\sigma$ (99.5% confidence interval), that is, $\Delta\nu_{1/2} = 6\sigma$. $\Delta\nu_{1/2}$(basic) is equal to the line widths in the indirect dimensions of conventional FT NMR spectra recorded with the same maximal evolution time (Figures 6e, 7; see text). Hence, σ(basic) likewise represents the standard deviation obtained in FT NMR. Correspondingly are $\sigma(\text{second}) = \Delta\nu_{1/2}(\text{second})/6$ and $\sigma(\text{third}) = \Delta\nu_{1/2}(\text{third})/6$ the standard deviations for peak position identification in *B*13 and *B*14, and *B*15. The deviations $\sigma(^1H^{\alpha})$, $\sigma(^{13}C^{\alpha})$, $\sigma(^{13}C')$, and $\sigma(^{15}N)$ were obtained from Monte Carlo simulations of error propagation for which the following systems of equations were considered: (i) a minimal number of four out of the eight basic spectra (*B*1, *B*4, *B*6, *B*7; Figure S1), (ii) *B*1−*B*8, (iii) *B*1−*B*12, (iv) *B*1−*B*14, or (v) *B*1−*B*15. Peak positions were randomly varied 10 000 times according to Gaussian distributions characterized by σ(basic), σ(second), and σ(third). Subsequently, the systems of equations were solved using a least-squares fitting routine, and the deviations among the 10 000 solutions yielded $\sigma(^1H^{\alpha})$, $\sigma(^{13}C^{\alpha})$, $\sigma(^{13}C')$, and $\sigma(^{15}N)$. Note that $\sigma(^1H^{\alpha})$ is not further reduced when central peaks are involved because those do not encode $\Omega(^1H^{\alpha})$. Similarly, $\sigma(^{13}C^{\alpha})$ and $\sigma(^{13}C')$ are not further reduced when second- and third-order central peaks are considered for calculation of chemical shifts. Notably, the standard deviations (labeled with an asterisk) obtained with four spectra critically depend on the particular selection (Figure S1). The highest precision is obtained when choosing either *B*1, *B*4, *B*6, and *B*7, or *B*2, *B*3, *B*5, and *B*8 (Figures S1, 6). The simulations are in neat agreement with calculations using the Gaussian law of error propagation[8] (see Figure S1 in the Supporting Information).

than ubiquitin at 25 °C that the precision of the indirectly detected shifts will be higher than that for the directly detected amide proton shift. This is because the precision of shift measurements in the indirect constant-time evolution periods is determined[11] by t_{max} (which would not change for larger proteins), while the precision in the direct dimension is decreasing with increasing $R_{2,HN}$.

Conclusions

GFT NMR relaxes on constraints arising from two major drawbacks of FT NMR, that is, the problem of having excessive or prohibitively long measurement times due to sampling of indirect dimensions and the limited precision of chemical shift measurements in the indirect dimensions arising from comparably low digital resolution. Within a few hours or less, GFT NMR affords the correlations of even five- or higher-dimensional FT NMR spectra acquired with high digital resolution. Thus, GFT NMR allows one to tune measurement times to sensitivity requirements without compromising on the dimensionality or the digital resolution. High-throughput efforts such as NMR-based structural genomics[13] will profit from this feature because automated resonance assignment[6i,14] benefits from maximizing the number of correlations obtained in a single NMR experiment. Moreover, the rapid sampling realized with GFT NMR will allow researchers to obtain highest dimensional NMR information with exceptional time resolution when, for example, studying slow protein folding in real time.[15] The high precision of the chemical shift measurements is of potential importance for a broad range of NMR applications in natural sciences and engineering, for example, for automated assignment, or when studying systems with high chemical shift degeneracy such as RNA ribose spin systems,[16] (partially) unfolded proteins,[17] or lipids.[18] Finally, the high precision of

(13) Montelione, G. T.; Zheng, D.; Huang, Y. J.; Gunsalus, K. C.; Szyperski, T. *Nat. Struct. Biol.* **2000**, *7*, 982−984.
(14) (a) Moseley, H. N. B.; Montelione, G. T. *Curr. Opin. Struct. Biol.* **1999**, *9*, 635−642. (b) Moseley, H. N. B.; Monleon, D.; Montelione, G. T. *Methods Enzymol.* **2001**, *339*, 91−108.
(15) Dyson, H. J.; Wright, P. E. *Annu. Rev. Phys. Chem.* **1996**, *47*, 369−395.
(16) Cromsigt, J.; van Buuren, B.; Wijmenga, S. *Methods Enzymol.* **2001**, *338*, 371−399.
(17) Neri, D.; Wider, G.; Wüthrich, K. *FEBS Lett.* **1992**, *303*, 129−135.
(18) Wang, H.; He, Y.; Kroenke, C. D.; Kodukula, S.; Storch, J.; Palmer, A. G.; Stark, R. E. *Biochemistry* **2002**, *41*, 5453−5461.

theshift measurements may be recruited to accurately measure other NMR parameters such as residual dipolar couplings for structural refinement,[19] and transverse relaxation optimized[20] GFT NMR may develop into a powerful approach to investigate larger systems.

Acknowledgment. Support was provided by the University at Buffalo, the National Science Foundation (MCB 0075773), and the National Institutes of Health (The Northeast Structural Genomics Consortium; P50 GM62413-01). We thank Drs. G. Montelione, Rutgers University, and F. Bright, University at Buffalo, for helpful discussions, Drs. John Cort and Michael Kennedy, Pacific Northwest National Laboratories, for providing the sample of $^{13}C/^{15}N$-labeled ubiquitin, and Mr. Yang Shen for help in preparing Figure 8.

Supporting Information Available: I. Detailed description of frequency domain editing of chemical shift multiplets and relation to the formalism for time domain editing. II. Options to implement central peak acquisition in GFT NMR. III. Formula to calculate the reductions in minimal measurement times for different options for central peak acquisition. IV. Details of processing the (5,2)D HACACONHN GFT NMR spectrum. V. Table S1 with reductions in minimal measurement times in GFT NMR. VI. Table S2 with ^{1}H, ^{15}N, and ^{13}C chemical shifts of ubiquitin obtained from (5,2)D HACACONHN GFT NMR. VII. Figure S1 showing additional results of Monte Carlo simulations related to Figure 8, as well as analytical calculations of error propagation (PDF). This material is available free of charge via the Internet at http://pubs.acs.org.

JA028197D

(19) (a) Tjandra, N.; Bax, A. *Science* **1997**, *278*, 1111−1114. (b) Prestegard, J. H. *Nat. Struct. Biol.* **1998**, *5*, 517−522.
(20) Pervushin, K.; Riek, R.; Wider, G.; Wüthrich, K. *Proc. Natl. Acad. Sci. U.S.A.* **1997**, *94*, 12366−12371.
(21) Kay, L. E.; Keifer, P.; Saarinen, T. *J. Am. Chem. Soc.* **1992**, *114*, 10663−10665.